ACS APPLIED MATERIALS & INTERFACES

Research Article

www.acsami.org

One-Pot Synthesis of Magnetic Ni@$Mg(OH)_2$ Core–Shell Nanocomposites as a Recyclable Removal Agent for Heavy Metals

Meng Zhang,* Weiqiang Song, Qiuling Chen, Baoji Miao, and Weichun He

School of Materials Science and Engineering, Henan University of Technology, Zhengzhou, 450007, P. R. China

Supporting Information

ABSTRACT: A surfactant-assisted hydrothermal route has been presented to one-pot synthesized Ni nanoparticles encapsulated in $Mg(OH)_2$ hollow spheres. The diameter of Ni cores and the thickness of $Mg(OH)_2$ shells are about 60–80 and 15 nm, respectively, and the size of a whole composite sphere is approximately 70–100 nm. Benefiting from the ferrimagnetic behavior of Ni cores and the high surface area of $Mg(OH)_2$ shells, Ni@$Mg(OH)_2$ nanocomposites exhibit excellent heavy metals adsorption capacity and recyclable property. The first removal efficiency is almost 100% for target metals, and after five cycles, the adsorption capacity remains 95%. A series of experiments show the adsorption of heavy metal ions on Ni@$Mg(OH)_2$ follows a pseudo-second order kinetic equation and can be described by a Langmuir isotherm model.

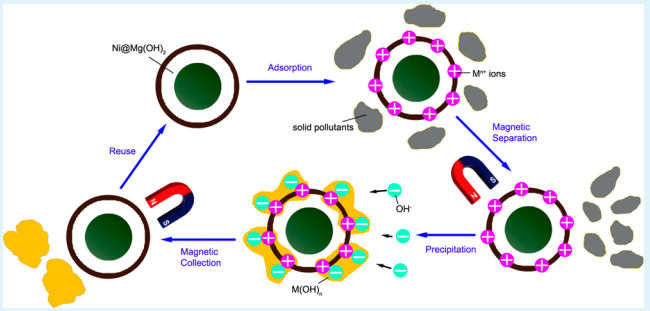

KEYWORDS: *Ni@$Mg(OH)_2$ nanocomposites, one-pot synthesis, magnetic separation, heavy metal wastewater, recyclability*

1. INTRODUCTION

Water pollution caused by heavy metals is one of the serious worldwide environmental issues.[1−5] Because of environmental friendliness, high adsorption capacity, and thermal stability, $Mg(OH)_2$ has been considered as an ideal water treatment agent to remove heavy metals, including nickel, cobalt, lead, copper, zinc, and cadmium.[6−9] However, the conventional $Mg(OH)_2$ water treatment agent has to suffer from poor recyclability. For example, the wastewater often contain some solid pollutants, which always mix together with the $Mg(OH)_2$ particles, and it is difficult to separate $Mg(OH)_2$ from the mixture.

Recently, magnetic nanoparticles have stimulated extensive studies because of their promising applications in diverse fields such as magnetic recording media,[10−12] magnetic sensors,[13,14] magnetic resonance imaging contrast agents,[15] magnetic targeted drug delivery,[16] and magnetic separation.[17] Among these applications, the magnetic separation inspires us to develop a magnetic selective collection strategy. In this strategy, Ni@$Mg(OH)_2$ core–shell composite nanostructures have been synthesized as a recyclable water treatment agent. Making use of the magnetism of Ni core, we successfully separate and collect the Ni@$Mg(OH)_2$ nanocomposites from the mixture under an external magnetic field and eventually achieve the water treatment agent reuse. It should be mentioned that nanosized Ni particles are easily oxidized to NiO by air and lose the magnetism.[17,18] Herein, the $Mg(OH)_2$ shell is equal to a protective layer, which can prevent the Ni core from oxidizing and keep the magnetism.

2. EXPERIMENTAL SECTION

2.1. Synthesis of Ni@$Mg(OH)_2$ Core–Shell Nanocomposites. In a typical procedure, 0.45 g of poly(vinylpyrrolidone) (PVP, K-30) was first introduced into 45 mL of hexane/water (volume ratio was 8:1) system with agitation. Then 2.5 mmol of $NiCl_2 \cdot 6H_2O$, 2 mL of $NH_3 \cdot H_2O$, and 2.5 mmol Mg powder were added into the above emulsion, respectively. After stirring for a few minutes, the mixture was transferred into a Teflon-lined stainless steel autoclave and kept at 200 °C for 20 h and then cooled to room temperature naturally. The product was centrifuged and washed with distilled water and absolute ethanol several times, until a black precipitate was collected. Finally, the obtained product was dried in vacuum at 50 °C for 6 h.

2.2. Characterization. The phase purity and crystal structure of the product were detected by powder X-ray diffraction (XRD; Phillips X'Pert SUPER) with Cu Kα radiation (λ = 1.5418 Å). The morphology was observed by a transmission electron microscope (TEM; Hitachi 800), using an accelerating voltage of 200 kV. Further detailed structural characterization and the elemental composition analysis were performed on a high-resolution TEM (HRTEM; JEOL-2010) equipped with an energy-dispersive X-ray (EDX, Oxford) spectrum, also at 200 kV. The content of Ni and $Mg(OH)_2$ were estimated by thermal gravimetric analysis (TGA; DT-50) in an argon atmosphere. Magnetic properties were measured on a MPMS XL-7 SQUID magnetometer. The specific surface area was evaluated from nitrogen adsorption data (ASAP 2010). The surface charges were examined with a Nanotrac Wave zeta potential analyzer.

2.3. Heavy Metals Removal Experiments. To test the effect of Ni@$Mg(OH)_2$ nanocomposites on removing heavy metals, the solution

Received: September 30, 2014
Accepted: January 5, 2015
Published: January 5, 2015

DOI: 10.1021/am506643b
ACS Appl. Mater. Interfaces 2015, 7, 1533−1540

Scheme 1. Synthetic Procedure of Ni@Mg(OH)$_2$ Core−Shell Composite Nanostructures

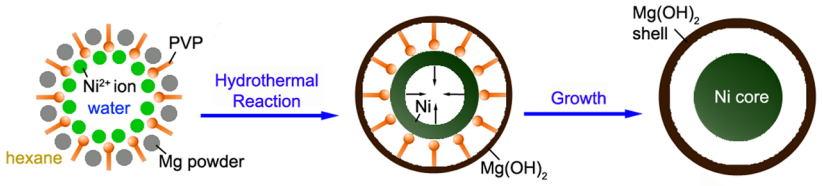

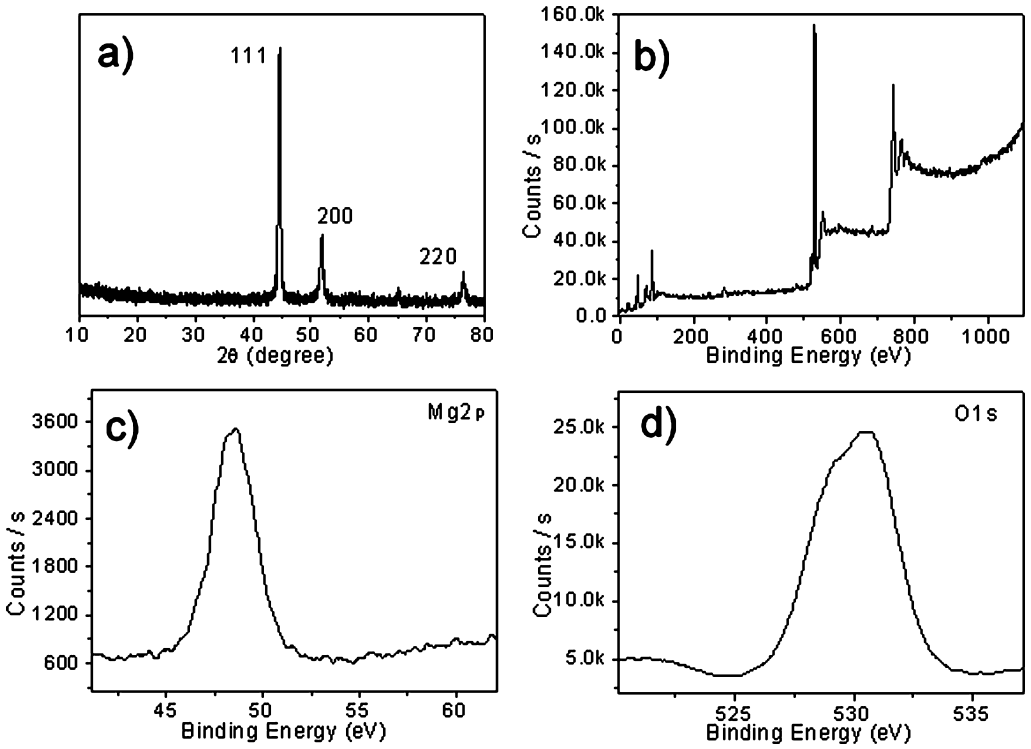

Figure 1. (a) XRD patterns and (b−d) XPS spectra of as-prepared Ni@Mg(OH)$_2$.

contains Zn^{2+}, Cd^{2+}, and Cu^{2+}, and kaolin (simulating solid pollutants) were prepared at room temperature. In a representative solution, the concentrations of three metal ions and kaolin were 90 mg L^{-1} (30 mg L^{-1} for each) and 3 g L^{-1}, and the pH value was adjusted to ~6.5. After 60 min, the concentrations of Zn^{2+}, Cd^{2+}, and Cu^{2+} were determined by atomic absorption spectroscopy (AAS; AAanlyst 800), and the values are 28.3, 28.8, and 28.5 mg L^{-1}, respectively. The decrease of heavy metal ions came from the adsorption of kaolin. Then, 0.2 g of Ni@Mg(OH)$_2$ nanocomposites were put into the above 50 mL solution at room temperature for 60 min under continuous stirring conditions.

3. RESULTS AND DISCUSSION

3.1. Formation Mechanism of Ni@Mg(OH)$_2$ Core−Shell Nanocomposites. Scheme 1 illustrates the synthesis process of Ni@Mg(OH)$_2$ nanocomposites. The PVP molecules possess hydrophobic (alkyl) and hydrophilic (oxygen atoms) groups as well, so PVP can bridge hexane and water at their interface and form a water/hexane emulsion.[19,20] When the ratio between hexane and water was in an appropriate range, nanoscale water droplets were obtained and dispersed in hexane through agitation. Theses water droplets provided a constant environment for the nanoparticles growth. Ni^{2+} ions readily dissolved in these water droplets owing to the strong affinity of the PVP oxygen atoms for Ni^{2+} ions. Under hydrothermal conditions, Ni^{2+} ions were reduced to Ni atoms by Mg powder:

$$Mg + Ni^{2+} \rightarrow Mg^{2+} + Ni \quad (1)$$

At the same time, Mg^{2+} ions (rooting in eq 1) reacted with $NH_3{\cdot}H_2O$ to form Mg(OH)$_2$, which deposited on the surface of water droplets and gradually accumulated into shells. The Mg(OH)$_2$ shells blocked the outward growth of Ni nanoparticles and ultimately creating Ni@Mg(OH)$_2$ nanocomposites.

To confirm the above mechanism, we performed a control experiment with a short reaction time of 5 h, and found the intermediates were mainly Ni hollow spheres (see Supporting Information Figure S1), which are convincing evidence that the nascent Ni forms on the inner wall of water droplets. Prolonging the reaction time, these hollow spheres would grew inward to solid spheres and served as cores of Ni@Mg(OH)$_2$ nanocomposites.

Additionally, $NH_3{\cdot}H_2O$ also played an important role in the formation of Ni@Mg(OH)$_2$ nanocomposites. In our reaction system, Ni^{2+} ions complexed with $NH_3{\cdot}H_2O$ to form $[Ni(NH_3)_4]^{2+}$ in solution:

$$Ni^{2+} + 4NH_3{\cdot}H_2O \rightarrow [Ni(NH_3)_4]^{2+} + 4H_2O \quad (2)$$

With a rise in temperature, $[Ni(NH_3)_4]^{2+}$ would slowly release free Ni^{2+} ions to take part in the reduction reaction (eq 1). In place of $NH_3{\cdot}H_2O$ with other base (e.g., NaOH), only irregular nanoparticles were obtained. That demonstrates a relatively low concentration of free Ni^{2+} ions is able to slow down the reaction rate and control the nucleation and growth well, which are

DOI: 10.1021/am506643b
ACS Appl. Mater. Interfaces 2015, 7, 1533−1540

essential for the shaping of Ni@$Mg(OH)_2$ nanocomposites. The whole reaction can be summarized as eq 3:

$$NiCl_2 + Mg + 2NH_3{\cdot}H_2O \rightarrow Ni + Mg(OH)_2 + 2NH_4Cl \quad (3)$$

3.2. Characterization of Ni@$Mg(OH)_2$ Core−Shell Nanocomposites. Figure 1a shows the XRD pattern of the products prepared through the typical process. All of the reflection peaks can be easily indexed to a face-centered cubic phase [space group *Fm*3*m* (225)] of nickel. The calculated cell constant is a = 3.526 Å, which is close to the literature value (JCPDS card no. 04-0850; a = 3.523 Å). Besides, no diffraction peak of $Mg(OH)_2$ can be distinctly identified. This result seems to suggest that the shells mainly consist of amorphous $Mg(OH)_2$.

To ascertain the composition of the shells, we have employed the XPS technique, which can analyze the composition of the surface layer of the compound with a depth penetration of approximately 2−3 nm. The survey XPS spectrum of the product is illustrated in Figure 1b. The binding energies obtained in the XPS analysis are standardized for specimen charging using C 1s as the reference at 284.57 eV. No other elements except Mg, O, Ni, and C are observed in the spectrum. The characteristic peaks for Mg 2p and O 1s are at 48.98 and 530.67 eV, respectively (Figure 1c,d), which are consistent with the previously published XPS spectrum of $Mg(OH)_2$. It is worth mentioning that XPS analysis can hardly detect any Ni 2p signal, which confirms that the Ni nanoparticles are mostly encapsulated inside the amorphous $Mg(OH)_2$ shells. The EDX spectra present the further composition information on Ni@$Mg(OH)_2$ nanocomposites (see the Supporting Information, Figure S2).

As shown in Figure 2a, a high yield of spherical core−shell nanostructures can be clearly observed. The sizes of Ni cores are distributed over the range of 60−80 nm in diameter. There is a $Mg(OH)_2$ shell with ∼15 nm in thickness around the Ni core. These nanocomposites are inclined to accumulate together because of their magnetism. The enlarged TEM image indicates that an individual nanosphere (Figure 2b), whose core region is darker than the shell part, meaning that the core and shell have different components.

To investigate the structural details of Ni cores, HRTEM studies were performed taken from uncovered Ni nanoparticles (in the inset of Figure 2c). An intersecting lattice structure was demonstrated in Figure 2c. One interplanar spacing is 0.106 nm, and another is 0.123 nm. There are still well-resolved lattice planes near the particle edge (top right corner), implying that the Ni nanoparticles possess high crystallinity and structurally uniform. The SAED pattern can be indexed for the [1$\bar{2}$3] zone axis of Ni (Figure 2d), in which pattern spots can be clearly seen whose presence exhibits the single crystalline nature of the selected area.

The TGA curve of Ni@$Mg(OH)_2$ nanocomposites is displayed in Figure 3a. The distinct weight loss that happens between 337 and 411 °C may be attributed to the dehydration of magnesium hydroxide: $Mg(OH)_2 \rightarrow MgO + H_2O$. This dehydration process causes a loss of 12.7 wt %. On the basis of this data, the $Mg(OH)_2$ content in nanocomposites is approximately estimated to be 40.9 wt %.

Figure 3b gives the room-temperature magnetic hysteresis loops of Ni@$Mg(OH)_2$ nanocomposites. The saturation magnetization (M_s) is 39.75 emu g^{-1}, which is less than that of bulk nickel.[21] This is because $Mg(OH)_2$ are not magnetic materials, thus pulling down the magnetization of Ni@$Mg(OH)_2$

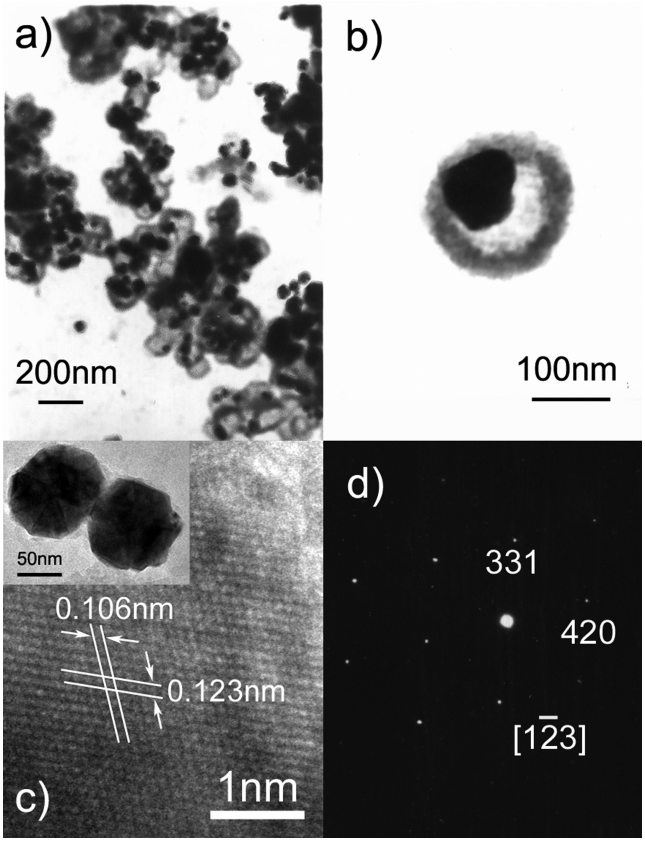

Figure 2. (a, b) TEM images of Ni@$Mg(OH)_2$ nanocomposites, (c) HRTEM images, and (d) SAED patterns of Ni cores.

nanocomposites. The coercivity (H_c) is up to 199 Oe, while the H_c value of bulk nickel is not more than 100 Oe.[22] The increase of coercivity reveals the size of Ni core is larger than the single-domain critical size of Ni. The above behavior displays typical ferromagnetic properties, which ensure Ni@$Mg(OH)_2$ nanocomposites can be readily collected via magnetic separation and repeatedly used as a removal agent.

The adsorption capability of Ni@$Mg(OH)_2$ nanocomposites was evaluated from N_2 adsorption/desorption isotherms (Figure 4a). The BET specific surface area and pore volumes were 124.2 $m^2\ g^{-1}$ and 0.15 $cm^3\ g^{-1}$, respectively. By using the BJH model, the pore size distribution was calculated and shown as an inset in Figure 4a. The pore diameters concentrated in the rages of 2−20 nm, and the average diameter was 5.5 nm, which indicated Ni@$Mg(OH)_2$ nanocomposites had mesoporous structures. These features are conducive to the adsorption of heavy metal ions from aqueous solutions.

The electrostatic attraction coming from the surface charges of particles is another important factor deciding the adsorption behavior.[23] To our knowledge, the surface charges are usually varied with the change of pH value, so we analyzed the zeta potential of Ni@$Mg(OH)_2$ nanocomposites at different pH conditions. As shown in Figure 4b, the zeta potential is positive at low pH values. Increasing the pH value, the zeta potential gradually becomes negative and reaches the maximum value of −12.6 mV while pH value increases to 6.5. This fact that negative charges are present on the surface of Ni@$Mg(OH)_2$ nanocomposites helps enhance the adsorption capacity for heavy metal ions through additional electrostatic attraction.

3.3. Heavy Metal Removal Efficiency and Recyclable Property. The recycling strategy of Ni@$Mg(OH)_2$ nano-

DOI: 10.1021/am506643b
ACS Appl. Mater. Interfaces 2015, 7, 1533−1540

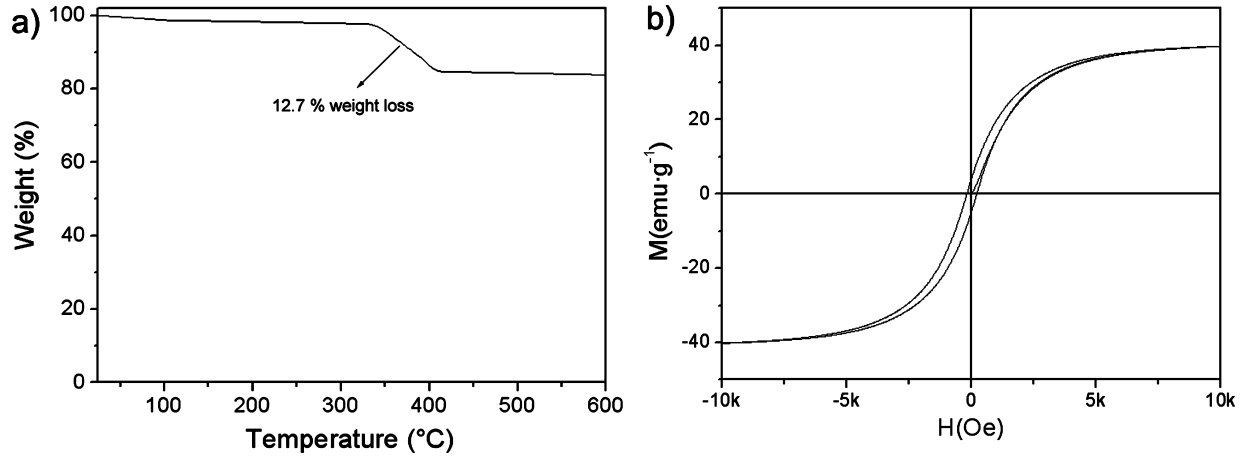

Figure 3. (a) TGA curve and (b) field-dependent magnetization of $Ni@Mg(OH)_2$ nanocomposites.

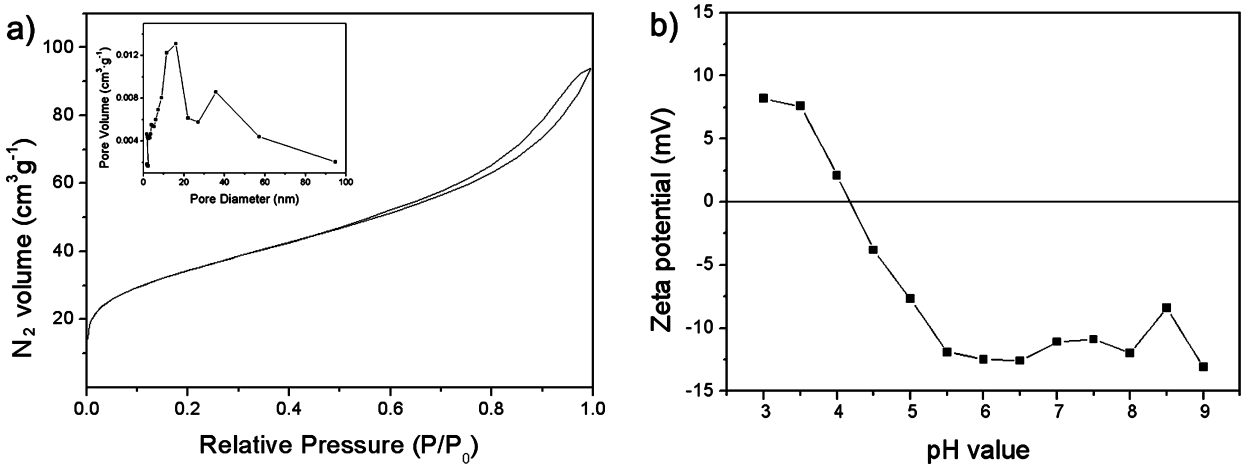

Figure 4. (a) N_2 adsorption/desorption isotherm, (inset of a) pore-size distribution and (b) zeta potential at different pH values of $Ni@Mg(OH)_2$ nanocomposites.

Scheme 2. Recycling Strategy of $Ni@Mg(OH)_2$ Water Treatment Agent

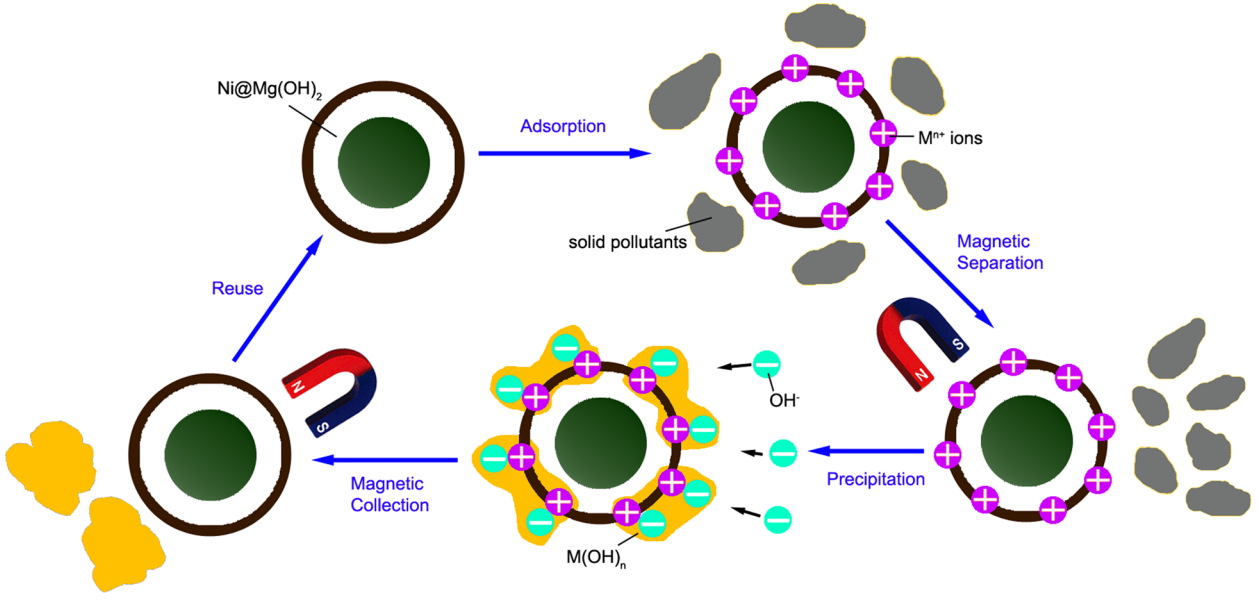

composites is shown in Scheme 2. First, $Ni@Mg(OH)_2$ nanocomposites were introduced into wastewater to adsorb heavy metal ions (M^{n+}) and then separated from the mixture solution employing a magnet. Next, the adsorbed M^{n+} ions were

DOI: 10.1021/am506643b
ACS Appl. Mater. Interfaces 2015, 7, 1533−1540

desorbed from Ni@$Mg(OH)_2$ nanocomposites and precipitated as $M(OH)_n$ through washing them by alkaline solution. Finally, the recovered Ni@$Mg(OH)_2$ nanocomposites were magnetically collected and used again to remove heavy metals from wastewater. Moreover, the heavy metal may be also recycled in this strategy.

The heavy metal (selecting Zn^{2+}, Cd^{2+}, and Cu^{2+} ions as examples) removal efficacy of Ni@$Mg(OH)_2$ nanocomposites can be directly observed by the change of the color of the solution. After undergoing adsorption and magnetic separation, the solution turned from light greenish blue to colorless. There were still kaolin particles in solution, which meant Ni@$Mg(OH)_2$ nanocomposites/M^{n+} could be effectively separated from the mixture of solid pollutants.

The heavy metal removal efficiency (deducting the kaolin influence) is shown in Figure 5. The initial removal was complete

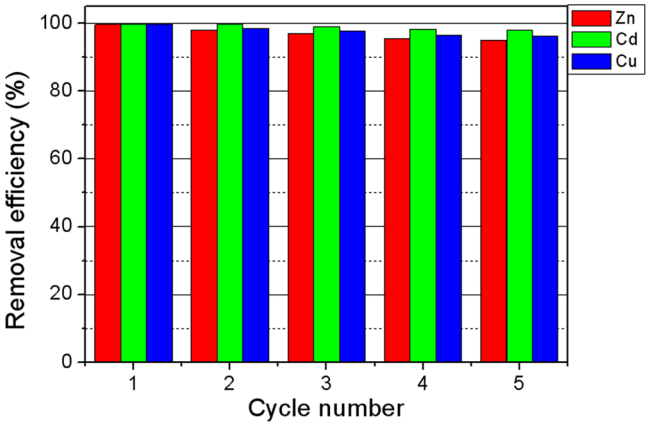

Figure 5. Heavy metal removal efficacy and recycling of Ni@$Mg(OH)_2$ nanocomposites.

with a high rate of almost 100%, which indicated Ni@$Mg(OH)_2$ nanocomposites were highly efficient adsorbents for heavy metal removal from solution. We repeatedly carried out the adsorption experiments and found the recovered Ni@$Mg(OH)_2$ nanocomposites possessed excellent removal efficiency retention during cycling. The removal efficiency maintained 95% after 5 cycles, and particularly Cd^{2+} removal efficiency consistently kept more than 98.1%. In our opinion, such a good reproducibility mainly results from the following two reasons. First, Ni@$Mg(OH)_2$ nanocomposites have mesoporous structures. The porosity accommodates the volume changes induced by the adsorption and desorption of M^{n+} ions so that Ni@$Mg(OH)_2$ sustain their architectures and adsorption capability. Second, $Mg(OH)_2$ shells slow down the oxidation of Ni cores and thus maintain their magnetic properties upon cycling.

3.4. Adsorption Kinetics. Figure 6 shows the adsorption of Zn^{2+}, Cd^{2+}, and Cu^{2+} (initial concentration of 30 mg L^{-1} for each; without kaolin) on Ni@$Mg(OH)_2$ as a function of contact time. All the three ions had similar adsorption trends. The removal efficiency rose sharply within the beginning 20 min and subsequently increased slowly close to 100% after 30−40 min; afterward, the removal efficiency no longer changed even the contact time extended to 120 min (Figure 6a). We think the initial high removal efficiency corresponds to the fast diffusion of M^{n+} ions from the solution to the adsorbent surfaces. The later low removal efficiency corresponds to the slow diffusion of M^{n+} ions from the adsorbent surfaces to inners or ion transfer at the interface between adsorbent particles.[24]

The adsorption capacity q can be defined as

$$q = \Delta cV/m \tag{4}$$

where Δc is the concentration change of M^{n+} (mg L^{-1}), V is the solution volume (L), and m is the mass of Ni@$Mg(OH)_2$ nanocomposites (g). According to eq 4, the adsorption capacities are calculated using the data rooting in the above experiment and shown in Figure 6b. As we know, the adsorption kinetics may be described by pseudo-first order and pseudo-second order kinetic models. Through modeling the experiment data during 50 min, we find the pseudo-second order model fit the adsorption of M^{n+} on Ni@$Mg(OH)_2$ nanocomposites better than the pseudo-first order model. The pseudo-second order equation can be written as

$$\frac{dq_t}{dt} = k_2(q_e - q_t)^2 \tag{5}$$

where q_e and q_t are adsorption capacity at equilibrium and time t (mg g^{-1}), respectively, and k_2 is pseudo-second-order rate constant (g mg^{-1} min^{-1}). After integrating at boundary conditions, eq 5 can be rearranged as follows:

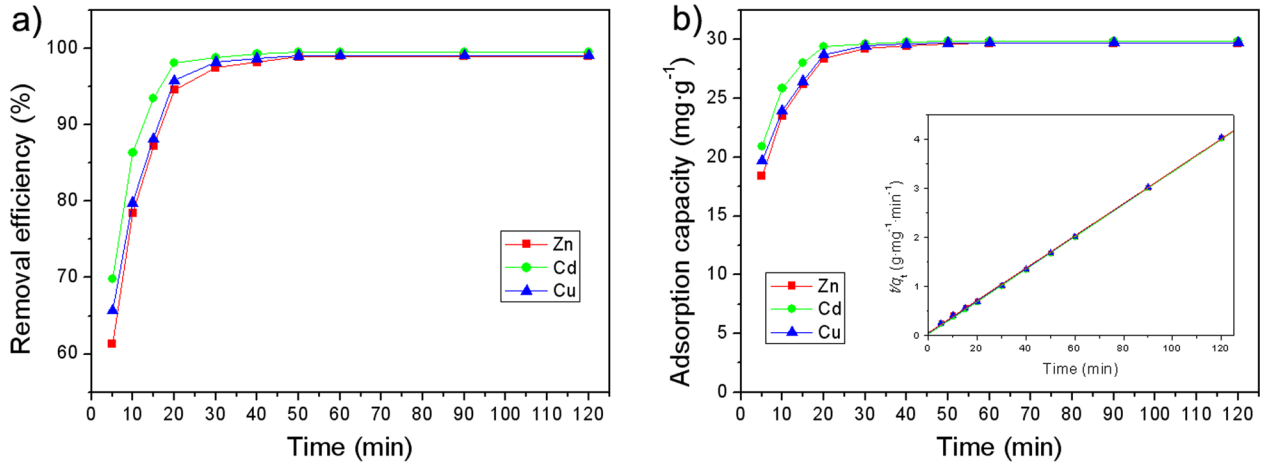

Figure 6. Effect of contact time on adsorption of heavy metal ions by Ni@$Mg(OH)_2$: (a) removal efficacy, (b) adsorption capacity, and (inset of b) pseudo-second order kinetics plots.

DOI: 10.1021/am506643b
ACS Appl. Mater. Interfaces 2015, 7, 1533−1540

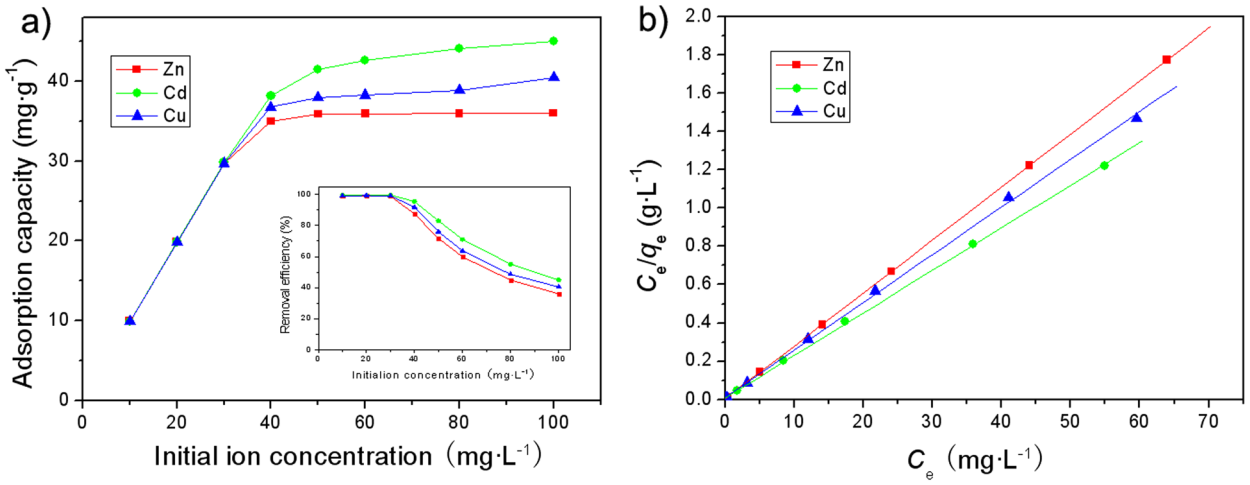

Figure 7. Effect of initial concentration on adsorption of heavy metal ions by Ni@$Mg(OH)_2$: (a) adsorption capacity, (inset of a) removal efficacy, and (b) Langmuir isotherm plots.

$$\frac{t}{q_t} = \frac{1}{k_2 q_e^{\ 2}} + \frac{t}{q_e} \quad (6)$$

The linear fitting based on eq 6 have been shown in the inset of Figure 6b. The value of k_2 and q_e for Zn^{2+}, Cd^{2+}, and Cu^{2+}, which can be obtained from the intercept and the slope of these linear plots, are 0.0161, 0.0283, and 0.019 g mg^{-1} min^{-1} and 30.42, 30.3, and 30.35 mg g^{-1}, respectively.

3.5. Adsorption Isotherm. Figure 7a shows the adsorption of Zn^{2+}, Cd^{2+}, and Cu^{2+} on Ni@$Mg(OH)_2$ as a function of their initial concentration (from 10 to 100 mg L^{-1} for each; without kaolin). One can see the equilibrium adsorption capacity of Ni@$Mg(OH)_2$ continuously rises with increasing the initial concentration of metal ions. When the initial concentration is increased to 100 mg L^{-1}, the equilibrium adsorption capacity for Zn^{2+}, Cd^{2+}, and Cu^{2+} are 36.03, 45.02, and 40.49 mg g^{-1}, respectively. The inset of Figure 7a illustrates the effect of the initial concentration of metal ions on the removal efficiency. All the three ions can be completely removed at 30 mg L^{-1} and lower initial concentration. With adjusting the initial concentration from 30 to 100 mg L^{-1}, the removal efficiency gradually decreases. This fact discloses metal ions fill the surface space of Ni@$Mg(OH)_2$ at the critical concentration,[25] so that the removal efficiency declines at higher concentration.

The Langmuir adsorption model has been employed to analyze the adsorption isotherms:

$$q_e = q_m \frac{KC_e}{1 + KC_e} \quad (7)$$

The linearized form of the Langmuir isotherm is given as

$$\frac{C_e}{q_e} = \frac{C_e}{q_m} + \frac{1}{Kq_m} \quad (8)$$

where q_m is the maximum adsorption capacity (mg g^{-1}), C_e is the equilibrium concentration of metal ions (mg L^{-1}), and K is the equilibrium constant (L mg^{-1}). Figure 7b gives the Langmuir isotherm. The relation between C_e/q_e and C_e appears a good linearity, so the adsorption of Zn^{2+}, Cd^{2+}, and Cu^{2+} on Ni@$Mg(OH)_2$ can be regarded as a monolayer adsorption process. According to eq 8, the maximum adsorption capacity for Zn^{2+}, Cd^{2+}, and Cu^{2+} are calculated to be 36.11, 44.98, and 40.18 mg g^{-1}, approximately the experimental values.

Comparing with other adsorbents (Table 1),[5,25−31] although some adsorbents have higher adsorption capacity for certain ions,

Table 1. Adsorption Capacity of Some Adsorbents for Zn^{2+}, Cd^{2+}, and Cu^{2+}

adsorbents	adsorption capacity for heavy metal ions (mg g^{-1})		
	Zn^{2+}	Cd^{2+}	Cu^{2+}
Purolite Arsen X^{np5}	4.84	8.2	5.57
magnetite nanorods[25]	55	46	40
magnetic modified chitosan[26]	32.16		
iron oxide coated sewage sludge[27]	42.4		17.3
iron oxide nanoparticles-immobilized-sand[28]		7.13	5.81
Fe_3O_4/ZnO/CuO nanoparticles[29]		31.5/51.3/42	11.5/148.5/6
dairy manure biochar[30]	51.4	32.8	54.4
activated charcoal derived from coffe[31]			38.2

such as Fe_3O_4 nanoparticles for Cu^{2+} and magnetite nanorods for Zn^{2+}, Ni@$Mg(OH)_2$ exhibit satisfactory adsorption for all three ions. Taking into account low cost, easy synthesis, and excellent recyclability, Ni@$Mg(OH)_2$ nanocomposites are more competitive in practical applications.

3.6. Practical Test. We collected the wastewater from an electroplate factory as a test sample to verify the real effect of Ni@$Mg(OH)_2$ removal agent. There are 7.5 mg L^{-1} Zn^{2+}, 20.5 mg L^{-1} Cd^{2+}, and 13.8 mg L^{-1} Cu^{2+} in the water sample. In our test system, 0.1 g of Ni@$Mg(OH)_2$ nanocomposites were put into a 50 mL water sample at room temperature. After agitating for 60 min, Ni@$Mg(OH)_2$ loaded with Zn^{2+}, Cd^{2+}, and Cu^{2+} were magnetically separated from the water sample. Then, they were washed by NaOH solution to release the adsorbed metal ions. The regenerated Ni@$Mg(OH)_2$ were magnetically collected and reused for 5 times. As shown in Figure 8, Ni@$Mg(OH)_2$ exhibited excellent removal efficiency and recyclability. The first removal efficiency for Zn^{2+}, Cd^{2+}, and Cu^{2+} ions reached 99.22%, 99.65%, and 99.49%, respectively. The adsorption capacity for the heavy metal ions only appeared slightly fading during cycling and the removal efficiency for Zn^{2+}, Cd^{2+}, and Cu^{2+} maintained 94.53%, 97.31%, and 95.45% after 6 cycles. The above results indicate that Ni@$Mg(OH)_2$ is a

DOI: 10.1021/am506643b
ACS Appl. Mater. Interfaces 2015, 7, 1533−1540

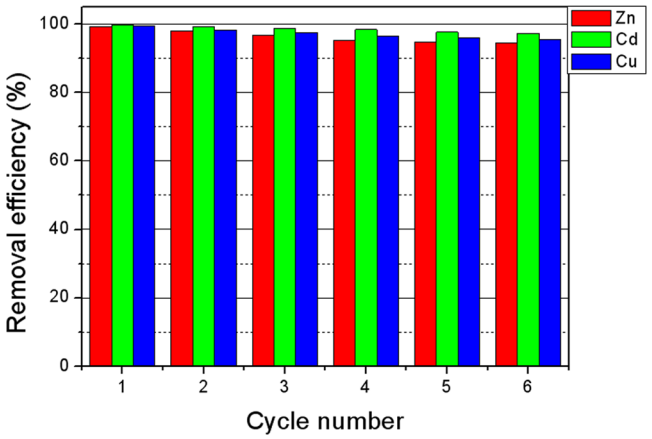

Figure 8. Practical test for heavy metal removal efficacy and recycling of Ni@$Mg(OH)_2$ nanocomposites (the water sample contained mixed Zn^{2+}, Cd^{2+}, and Cu^{2+} with an initial concentration of 7.5 mg L^{-1}, 20.5 mg L^{-1}, and 13.8 mg L^{-1}, respectively; pH value, ~ 6.3; temperature, 25 °C; adsorbent concentration, 2 g L^{-1}; contact time, 60 min).

promising recyclable water treatment agent in terms of high removal efficiency and low capacity loss.

CONCLUSIONS

In summary, Ni@$Mg(OH)_2$ core−shell nanocomposites were one-pot synthesized by a surfactant-assisted hydrothermal reduction method. Taking advantage of the high surface area and ferromagnetic properties of Ni@$Mg(OH)_2$ nanocomposites, we designed a magnetically recyclable strategy to remove the heavy metal from wastewater. This strategy ensured that adsorbent might be separated from the other solid pollutants. A series of experiments showed Ni@$Mg(OH)_2$ nanocomposites had high removal efficiency and low capacity fading. The practical test indicated that Ni@$Mg(OH)_2$ was an efficient recyclable water treatment agent, which was expected to clean up more types of wastewater.

ASSOCIATED CONTENT

Supporting Information

TEM image and XRD pattern of intermediates and EDX spectra of Ni@$Mg(OH)_2$ nanocompositse, Ni cores, and $Mg(OH)_2$ shells. This material is available free of charge via the Internet at http://pubs.acs.org.

AUTHOR INFORMATION

Corresponding Author

*E-mail: meng_zhang@haut.edu.cn.

Notes

The authors declare no competing financial interest.

ACKNOWLEDGMENTS

This work was supported by Zhengzhou Key Laboratory for Clean Energy (Grant 111PYFZX151) and Science and Technology Key Project from Education Department of Henan Province (Grant 13A150186).

REFERENCES

(1) Fu, F.; Wang, Q. Removal of Heavy Metal Ions from Wastewaters: A Review. *J. Environ. Manage.* **2011**, *92*, 407−418.
(2) Hashim, M. A.; Mukhopadhyay, S.; Sahu, J. N.; Sengupta, B. Remediation Technologies for Heavy Metal Contaminated Groundwater. *J. Environ. Manage.* **2011**, *92*, 2355−2388.
(3) Hua, M.; Zhang, S.; Pan, B.; Zhang, W.; Lv, L.; Zhang, Q. Heavy Metal Removal from Water/Wastewater by Nanosized Metal Oxides: A Review. *J. Hazard. Mater.* **2012**, *211−212*, 317−331.
(4) Gupta, V. K.; Ali, I.; Saleh, T. A.; Nayak, A.; Agarwal, S. Chemical Treatment Technologies for Waste-water Recycling—An Overview. *RSC Adv.* **2012**, *2*, 6380−6388.
(5) Kołodyńska, D.; Kowalczyk, M.; Hubicki, Z. Evaluation of Iron-based Hybrid Materials for Heavy Metal Ions Removal. *J. Mater.Sci.* **2014**, *49*, 2483−2495.
(6) Liu, W.; Huang, F.; Wang, Y.; Zou, T.; Zheng, J.; Lin, Z. Recycling $Mg(OH)_2$ Nanoadsorbent during Treating the Low Concentration of Cr^{VI}. *Environ. Sci. Technol.* **2011**, *45*, 1955−1961.
(7) Wang, Y.; Chen, J.; Lu, L.; Lin, Z. Reversible Switch between Bulk $MgCO_3{\cdot}3H_2O$ and $Mg(OH)_2$ Micro/Nanorods Induces Continuous Selective Preconcentration of Anionic Dyes. *ACS Appl. Mater. Interfaces* **2013**, *5*, 7698−7703.
(8) Li, C.; Zhang, Z.; Huang, F.; Wu, Z.; Hong, Y.; Lin, Z. Recycling Rare Earth Elements from Industrial Wastewater with Flowerlike Nano-$Mg(OH)_2$. *ACS Appl. Mater. Interfaces* **2013**, *5*, 9719−9725.
(9) Jia, B. B.; Wang, J. N.; Wu, J.; Li, C. J. Flower-Like" PA6@ $Mg(OH)_2$ Electrospun Nanofibers with Cr (VI)-Removal Capacity. *Chem. Eng. J.* **2014**, *254*, 98−105.
(10) Grobis, M.; Schulze, C.; Faustini, M.; Grosso, D.; Hellwig, O.; Makarov, D.; Albrecht, M. Recording Study of Percolated Perpendicular Media. *Appl. Phys. Lett.* **2011**, *98*, 192504.
(11) Ashiq, M. N.; Naz, F.; Malana, M. A.; Gohar, R. S.; Ahmad, Z. Role of Co−Cr Substitution on the Structural, Electrical and Magnetic Properties of Nickel Nano-ferrites Synthesized by the Chemical Co-precipitation Method. *Mater. Res. Bull.* **2012**, *47*, 683−686.
(12) Wu, L.; Jubert, P. O.; Berman, D.; Imaino, W.; Nelson, A.; Zhu, H.; Zhang, S.; Sun, S. Monolayer Assembly of Ferrimagnetic $Co_xFe_{3-x}O_4$ Nanocubes for Magnetic Recording. *Nano Lett.* **2014**, *14*, 3395−3399.
(13) Yang, Y.; Lin, L.; Zhang, Y.; Jing, Q.; Hou, T. C.; Wang, Z. L. Self-Powered Magnetic Sensor Based on a Triboelectric Nanogenerator. *ACS Nano* **2012**, *6*, 10378−10383.
(14) Koelle, D. Magnetic Sensors: A tip for Better Sensing. *Nat. Nanotechnol.* **2013**, *8*, 617−618.
(15) Lee, N.; Hyeon, T. Designed Synthesis of Uniformly Sized Iron Oxide Nanoparticles for Efficient Magnetic Resonance Imaging Contrast Agents. *Chem. Soc. Rev.* **2012**, *41*, 2575−2589.
(16) Veiseh, O.; Gunn, J. W.; Zhang, M. Design and Fabrication of Magnetic Nanoparticles for Targeted Drug Delivery and Imaging. *Adv. Drug Delivery Rev.* **2010**, *62*, 284−304.
(17) Kim, J.; Piao, Y.; Lee, N.; Park, Y. I.; Lee, I. H.; Lee, J. H.; Paik, S. R.; Hyeon, T. Magnetic Nanocomposite Spheres Decorated with NiO Nanoparticles for a Magnetically Recyclable Protein Separation System. *Adv. Mater.* **2010**, *22*, 57−60.
(18) Dutta, D.; Borah, B. J.; Saikia, L.; Pathak, M. G.; Sengupta, P.; Dutta, K. D. Synthesis and Catalytic Activity of Ni°-acid Activated Montmorillonite Nanoparticles. *Appl. Clay Sci.* **2011**, *53*, 650−656.
(19) Zhang, M.; Yan, G.; Hou, Y.; Wang, C. Mesoscale Assembly of NiO Nanosheets into Spheres. *J. Solid State Chem.* **2009**, *182*, 1206−1210.
(20) Khurana, J. M.; Vij, K. Nickel Nanoparticles Catalyzed Knoevenagel Condensation of Aromatic Aldehydes with Barbituric Acids and 2-thiobarbituric Acids. *Catal. Lett.* **2010**, *138*, 104−110.
(21) Hwang, J. H.; Dravid, V. P.; Teng, M. H.; Host, J. J.; Elliott, B. R.; Johnson, D. L.; Mason, T. O. Magnetic Properties of Graphitically Encapsulated Nickel Nanocrystals. *J. Mater. Res.* **1997**, *12*, 1076−1082.
(22) Sun, X. C.; Dong, X. L. Magnetic Properties and Microstructure of Carbon Encapsulated Ni Nanoparticles and Pure Ni Nanoparticles Coated with NiO Layer. *Mater. Res. Bull.* **2002**, *37*, 991−1004.
(23) Llorente, I.; Fajardo, S.; Bastidas, J. M. Applications of Electrokinetic Phenomena in Materials Science. *J. Solid State Electrochem.* **2014**, *18*, 293−307.

DOI: 10.1021/am506643b
ACS Appl. Mater. Interfaces 2015, 7, 1533−1540

(24) Zhao, D.; Sheng, G.; Hu, J.; Chen, C.; Wang, X. The Adsorption of Pb(II) on Mg_2Al Layered Double Hydroxide. *Chem. Eng. J.* **2011**, *171*, 167−174.
(25) Karami, H. Heavy Metal Removal from Water by Magnetite Nanorods. *Chem. Eng. J.* **2013**, *219*, 209−216.
(26) Fan, L.; Luo, C.; Lv, Z.; Lu, F.; Qiu, H. Preparation of Magnetic Modified Chitosan and Adsorption of Zn^{2+} from Aqueous Solutions. *Colloids Surf., B* **2011**, *88*, 574−581.
(27) Phuengprasop, T.; Sittiwong, J.; Unob, F. Removal of Heavy Metal Ions by Iron Oxide Coated Sewage Sludge. *J. Hazard. Mater.* **2011**, *186*, 502−507.
(28) Lee, S. M.; Laldawngliana, C.; Tiwari, D. Iron Oxide Nanoparticles-immobilized-sand Material in the Treatment of Cu (II), Cd (II) and Pb (II) Contaminated Waste Waters. *Chem. Eng. J.* **2012**, *195*, 103−111.
(29) Mahdavi, S.; Jalali, M.; Afkhami, A. Removal of Heavy Metals from Aqueous Solutions Using Fe_3O_4, ZnO, and CuO Nanoparticles. *J. Nanopart. Res.* **2012**, *14*, 1−18.
(30) Xu, X.; Cao, X.; Zhao, L.; Wang, H.; Yu, H.; Gao, B. Removal of Cu, Zn, and Cd from Aqueous Solutions by the Dairy Manure-derived Biochar. *Environ. Sci. Pollut. Res.* **2013**, *20*, 358−368.
(31) Yeung, P. T.; Chung, P. Y.; Tsang, H. C.; Tang, J. C. O.; Cheng, G. Y. M.; Gambari, R.; Chui, C. H.; Lam, K. H. Preparation and Characterization of Bio-safe Activated Charcoal Derived from Coffee Waste Residue and Its Application for Removal of Lead and Copper Ions. *RSC Adv.* **2014**, *4*, 38839−38847.

DOI: 10.1021/am506643b
ACS Appl. Mater. Interfaces 2015, 7, 1533−1540